Pupil-segmentation-based adaptive optical microscopy with full-pupil illumination

Daniel E. Milkie,[1] Eric Betzig,[2] and Na Ji[2,*]

[1]*Coleman Technologies, Inc., 5131 West Chester Pike, Newtown Square, Pennsylvania 19073, USA*

[2]*Janelia Farm Research Campus, Howard Hughes Medical Institute, 19700 Helix Dr., Ashburn, Virginia 20147, USA*

**Corresponding author: jin@janelia.hhmi.org*

Received July 15, 2011; revised September 20, 2011; accepted September 21, 2011;
posted September 26, 2011 (Doc. ID 150936); published October 25, 2011

Optical aberrations deteriorate the performance of microscopes. Adaptive optics can be used to improve imaging performance via wavefront shaping. Here, we demonstrate a pupil-segmentation based adaptive optical approach with full-pupil illumination. When implemented in a two-photon fluorescence microscope, it recovers diffraction-limited performance and improves imaging signal and resolution. © 2011 Optical Society of America

OCIS codes: 110.1080, 110.0180.

Because of the wave nature of light, the resolving power of conventional optical microscopy is limited by diffraction. In practice, however, diffraction-limited resolution is often not achieved because of optical aberrations [1]. For point-scanning microscopes such as a two-photon fluorescence microscope, the aberrations of the excitation light result in an enlarged focal spot within the sample and a deterioration of signal and resolution. Adaptive optics (AO) provides ways to recover the diffraction-limited performances by employing active optical components, such as a spatial light modulator (SLM), to modify the wavefront in such a way as to cancel out any existing aberrations [2,3]. Wavefront measurement in AO can be divided into two categories: those that use a sensor for direct measurement and those that deduce the wavefront indirectly from a series of images having different applied wavefront perturbations. For samples that strongly scatter light, the indirect method is preferred, because scattering scrambles the wavefront information.

Recently, we developed an image-based, indirect AO approach that is insensitive to sample scattering [4]. By comparing images of the sample taken with different zones or segments of the pupil illuminated one at a time, local tilt in the wavefront is measured from image shift. The complete aberrated wavefront is then obtained either by measuring the local phase offset directly using interference or via phase reconstruction algorithms similar to those used in astronomical AO. We implemented this pupil-segmentation-based approach in a two-photon fluorescence microscope and demonstrated that diffraction-limited resolution can be recovered from non-biological and biological samples [4,5].

This approach is zonal by nature, reminiscent of a Shack–Hartmann sensor in that it divides the wavefront into zones and measures the local tilt of each zone by image shift [2,3]. As with the Shack–Hartmann sensor, it works well with point sources or sparsely labeled samples. However, by illuminating only a small part of the pupil during the measurement process, each image is taken with a beamlet of much lower numerical aperture (NA) than that of the objective. As a result, the beamlet focus is greatly elongated, causing the resulting images to contain substantial contributions from fluorescent structures that were originally beyond the region of excitation under full-pupil illumination. For samples densely labeled in three dimensions, these additional structures make accurate image shift measurements very difficult.

We introduce here an extension of this method in which the full-pupil is illuminated during wavefront measurement. As before, it is based on a simple physical picture [4]: an ideal focus is formed when all light rays converge to a common point with a common phase [Fig. 1(a)]. Aberrations, however, deflect the rays such that they do not meet at a common spot and thus form an enlarged focus [Fig. 1(b)]. If we keep the wavefront fixed on all but one pupil segment and apply a series of phase ramps on this particular area, we effectively scan the light ray representing this area across this aberrated focus. Interference between this scanned ray and all the other fixed rays modulates the intensity of the signal collected from the focus. We visualize this modulation by plotting the signal relative to the scanning field position of the ray. If the scanned ray faces no aberrating

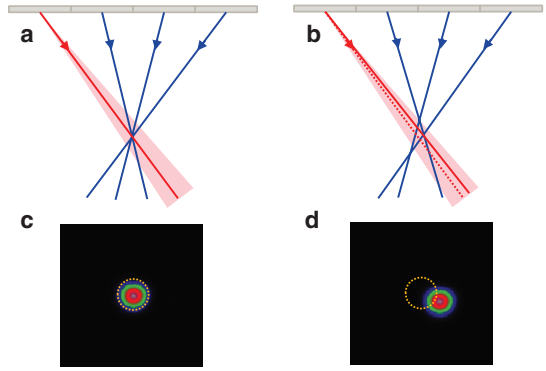

Fig. 1. (Color online) Schematic depicting the pupil-segmentation method with full-pupil illumination. (a) An ideal focus has all rays (blue and red) intersect at the same point, (b) whereas for an aberrated focus, rays do not. Scanning one of the rays (e.g., red ray) through a range of angles (shaded red cone) varies the intensity of the fluorescence excited at the focus. (c) Plotted as an image, this data exhibits an intensity extremum that is centered (dashed circle) over the scan region, provided the ray already intersects the ideal focus. (d) Shift of the extremum from the center indicates local wavefront tilt (dashed red line in b), which can be corrected by tilting the ray to the angle indicated by the extremum (solid red line in b).

 © 2011 Optical Society of America

inhomogeneities, this "image" (not a true image of the sample, but rather a map of the intensity variation of the focus) has a maximum at its center, corresponding to zero applied phase ramp [Fig. 1(c)]. Any wavefront perturbation, however, and the image takes on one of three forms: 1) a shifted maximum, if the scanned ray constructively interferes with the fixed rays [Fig. 1(d)]; 2) a shifted minimum, if this interference is destructive; and 3) relatively flat intensity, if the phase of the scanned ray relative to the fixed ones is near $\pm\pi/2$. In this latter case, an additional offset of $\pi/2$ is applied to the active pupil segment, and the measurement repeated, yielding an image with a shifted extremum. For any of the three scenarios, the displacement of the extremum indicates the local corrective wavefront tilt, as in a Shack–Hartmann sensor or our original pupil-segmentation algorithm. The same procedure is then sequentially applied to all segments across the entire rear pupil. After all wavefront tilts are measured, we can either directly measure the phase at each segment by stepping its phase and finding the value for maximal constructive interference or else reconstruct the complete wavefront algorithmically [4,6].

We have implemented this full-pupil illumination AO approach in a two-photon fluorescence microscope described previously [4]. Briefly, a liquid crystal SLM is conjugated to two galvanometer mirrors which scan the excitation focus across the sample. The SLM is conjugated to the back pupil plane of a 16×0.8 NA objective in order to manipulate the wavefront of the excitation. Initially, the phase offset for all pupil segments is set to zero. Then, for each segment in turn, phase ramps are applied that scan the corresponding ray across a $12\times12\,\mu m^2$ area around the focus, while at each scan position, the integrated signal from a $6\times6\,\mu m^2$ image of a fluorescent bead ($2\,\mu$m diameter) is recorded. The wavefront tilts for all segments where such scanning reveals a distinct extremum are then combined in a phase reconstruction algorithm [4,6] to find an overall corrective wavefront in these regions. For the remaining segments, where no extremum is observed, a phase offset of $\pi/2$, and then π, is applied, and the segment-by-segment scanning is repeated, until clear extrema are observed. The tilts for such segments are then combined with the previous ones to give the phase reconstruction over the entire rear pupil.

Figure 2 compares the full-pupil and single-segment illumination versions of our pupil-segmentation based AO approach. Two dimensional plots of the fluorescence signal versus the applied tilt at each segment are presented according to the segment's pupil location, similar to the array of spots projected onto a Shack–Hartman sensor. In the case where we first correct for system aberration and then apply full-pupil illumination AO, all segments exhibit maxima at the centers of their respective scan fields [Fig. 2(a)]. To test the corrective performance when faced with a realistic aberration, a wavefront previously measured during *in vivo* imaging in the mouse brain [5] is then applied to the SLM. With full-pupil illumination, the signal modulation is 5%–20% of the baseline level, as interference and nonlinear excitation both amplify the effect of a single-segment on the overall signal. The extrema show significant displacements from

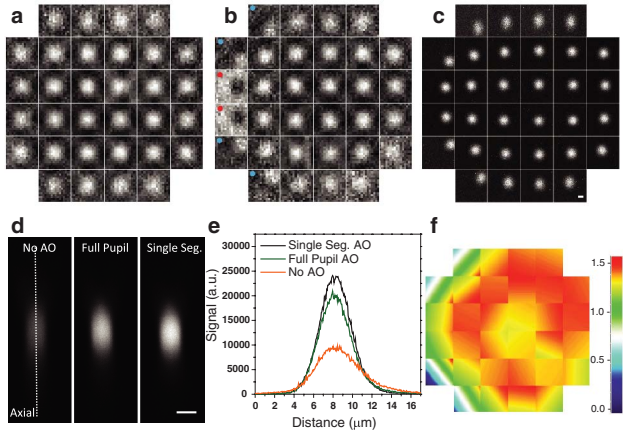

Fig. 2. (Color online) (a) For an aberration-free system under full-pupil illumination, the signal maximum for each pupil segment occurs at the center of its own scanned region. (b) Aberration causes the signal extremum for each segment to shift away from this center. Segments marked with red or blue dots were taken with $\pi/2$ or π initial phase offsets, respectively. (c) Images measured with single-segment illumination. (d) Axial images of a $2\,\mu$m diameter fluorescent bead without AO correction and with pupil-segmentation based AO under full-pupil and single-segment illumination, respectively. (e) The signal profile along the dotted line in (d). (f) The final corrective wavefront on the SLM obtained with full-pupil illumination, in wavelengths. Scale bar: $2\,\mu$m.

the center in several pupil segments [Fig. 2(b)] that match very well with the image displacements observed when only the active segment is illuminated [Fig. 2(c)]. Furthermore, axial images of fluorescent beads show

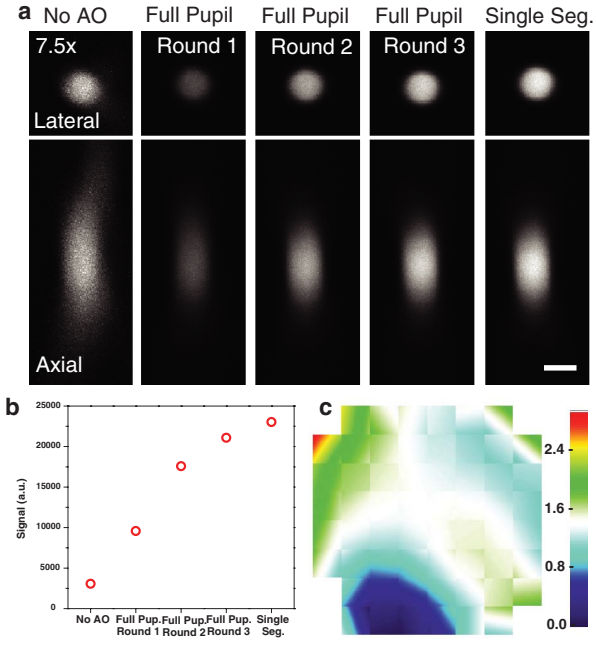

Fig. 3. (Color online) (a) Lateral and axial images of a $2\,\mu$m diameter bead without AO correction, with one, two, three rounds full-pupil illumination AO correction, and with single-segment illumination AO correction, respectively. The images without any AO correction (leftmost panel) have their intensity digitally enhanced 7.5× to aid visualization. (b) The maximal signal increases with iterative full-pupil illumination AO correction. (c) The corrective wavefront on the SLM, in wavelengths. Scale bar: $2\,\mu$m.

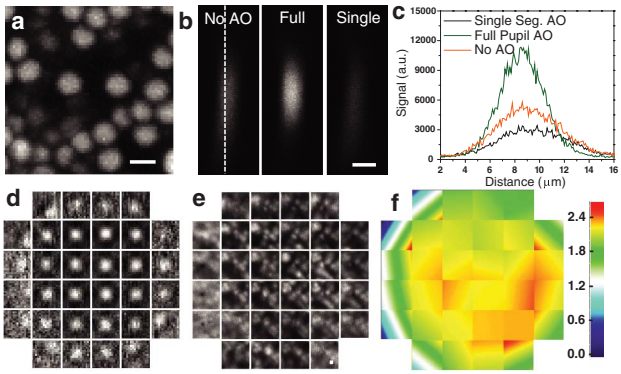

Fig. 4. (Color online) (a) Maximal intensity projection in 30 μm depth of a dense fluorescent bead sample. (b) Axial images of a 2 μm diameter bead without AO, with full-pupil illumination, and with single-segment illumination AO. (c) Signal profile along the dotted line in (b). (d) Signal modulation during full-pupil illumination AO. (e) Images measured with single-pupil illumination AO. (f) Aberration in unit of wavelength. Scale bar: 2 μm.

similar improvement in both signal and resolution for the full-pupil and single-segment illumination versions of pupil-segmentation based AO [Figs. 2(d) and 2(e)], while the corrective wavefront obtained with the full-pupil illumination closely matches the wavefront aberration as initially applied to the SLM [Fig. 2(f)].

Despite the similarity of the results, full-pupil illumination initially underperforms single-segment illumination during AO correction (e.g., lower signal in Fig. 2(e)]. This is due to the fact that, with full-pupil illumination, the ray from the active segment is interfering with a focal volume which itself is initially aberrated, so that the tilt at which the extremum is reached deviates from the tilt that would be measured if the focus from all the other rays were diffraction-limited. This deviation becomes increasingly significant for increasingly large initial aberration. For example, for the aberration in Fig. 3(c), one iteration with full-pupil illumination improves the signal 3×, whereas correction with single-segment illumination improves the signal 7.5×. However, with further iterations of the full-pupil algorithm, its performance is rapidly improved, since in successive iterations each ray is interfering with a progressively less aberrated focus. For the wavefront in Fig. 3, only two additional iterations are needed for the signal to approach that obtained using single-segment illumination [Figs. 3(a) and 3(b)].

One key advantage of using full-pupil illumination is that, by utilizing the whole NA of the microscope objective, the AO correction can be carried out under low excitation power. For example, in Fig. 3 the average power used for excitation at the sample ranges from 2 mW (3rd iteration) to 6 mW (1st iteration), while 16–25 mW of average power was used in the single-segment illumination case in order to compensate for the 8× reduction in excitation NA. This provides an important power margin for deep tissue imaging, where the excitation power is limited by scattering.

Another advantage is that full-pupil illumination extends our pupil-segmentation based AO approach to samples of arbitrary three-dimensional complexity, since the depth of focus during correction is much shorter than with single-segment illumination. For example, Fig. 4 shows AO correction of an applied aberration in a dense aggregation of 2 μm fluorescent beads in 3% agarose: correction with full-pupil illumination increases the signal 2×, whereas single-segment illumination yields an erroneous correction of reduced signal [Fig. 4(b)]. Analysis of the single-segment measurements in each case reveals why: the displacements of the extrema under full-pupil illumination can be measured unambiguously [Fig. 4(d)], whereas out-of-focus features lead to inaccurate displacement measurement under single-segment illumination [Fig. 4(e)].

Since our method relies on the intensity modulation of the focus, it is independent of image contrast mechanism, and thus can be applied to other imaging modalities, including linear fluorescence excitation, harmonic generation, sum-frequency generation, four-wave mixing, coherent anti-Stokes Raman scattering, stimulated Raman scattering, and stimulated emission depletion. Finally, pupil-segmentation with full-pupil illumination is potentially better suited to widefield AO, since all collected photons would be used in the correction, rather than just the small fraction impinging on one segment, as in our earlier implementation with single-segment illumination.

One current limitation of the full-pupil illumination approach is its speed, since the multiple tilts are applied to each pupil segment via the relatively slow SLM (20 Hz update rate), rather than the much faster galvo (2 kHz scan rate) used to tilt the active ray under single-segment illumination. However, new deformable mirrors with piston-tip-tilt segments and high update rates (>6.5 kHz) should improve the speed considerably [7].

The research is supported by the Howard Hughes Medical Institute.

References

1. M. J. Booth, Phil. Trans. R. Soc. A **365**, 2829 (2007).
2. R. K. Tyson, *Principles of Adaptive Optics* (Academic, 1991).
3. J. W. Hardy, *Adaptive Optics for Astronomical Telescopes* (Oxford University Press, 1998).
4. N. Ji, D. E. Milkie, and E. Betzig, Nat. Methods **7**, 141 (2010).
5. N. Ji, T. R. Sato, and E. Betzig, "Characterization and adaptive optical correction of aberrations during in vivo imaging in the mouse cortex," Proc. Acad. Natl. Sci. USA, submitted for publication.
6. S. I. Panagopoulou and D. R. Neal, J. Refract. Surg. **21**, S563 (2005).
7. M. A. Helmbrecht, M. He, C. J. Kempf, and M. Besse, Proc. SPIE **7931**, 793108 (2011).